Transport in Porous Media **2** (1987), 597–614.

Pore-Throat Size Correlation from Capillary Pressure Curves

N. C. WARDLAW
Department of Geology and Geophysics, University of Calgary, Calgary, Alberta T2N 1N4, Canada

Y. LI
Nanhi West Oil Corporation, P.O. Box 11, Potou, Zhanjiang, Guangdong, People's Republic of China

and

D. FORBES
Department of Geology and Geophysics, University of Calgary, Calgary, Alberta, T2N 1N4, Canada

(Received: 10 February 1987; revised: 29 July 1987)

Abstract. Void spaces in porous media can be considered as three-dimensional networks consisting of bulges (pores) connected by constrictions (throats). Computer simulations of drainage-imbibition processes show that the critical end points of wetting-phase and nonwetting-phase saturation, in drainage and imbibition respectively, and the form of simulated relative permeability curves all were significantly different for uncorrelated and correlated pore-throat models. Since these models were identical except for the arrangement of throats in relation to pores, the degree of pore-throat size correlation appears to be an important property influencing flow and fluid displacement. Examples of uncorrelated and correlated pore-throat structures in rocks are presented and it is shown that this property, although difficult to quantify by direct observation, can be evaluated from capillary pressure curves.

Key words: Drainage, imbibition, capillary pressure, pore, throat, relative permeability.

1. Introduction

Void spaces in porous media can be considered as three-dimensional networks consisting of bulges (pores) connected by constrictions (throats) (Figure 1). Where wetting and nonwetting fluids are present in the void spaces, the Laplace equation of capillarity relates the capillary pressures which are necessary for a nonwetting phase to penetrate throats or to withdraw from pores to the respective sizes of throats and pores.

Although the derivation of throat and/or pore size information from capillary pressure curves has been reported many times in the published literature (Purcell, 1949, 1950; Wardlaw and Taylor, 1976; Dullien, 1979; Bell *et al.*, 1981; Winslow and Lovell, 1981), little attention has been paid to the way in which pores and throats of different sizes are arranged relative to each other. Evidence has been presented that relative permeability and displacement efficiency both

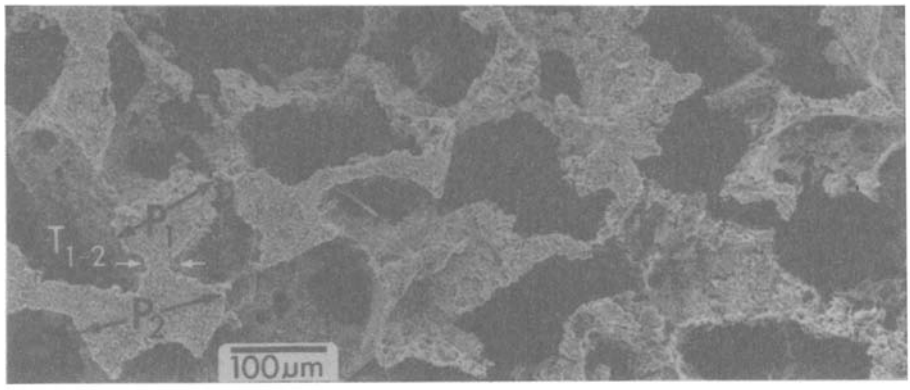

Fig. 1. Wood's metal occupying pore space in Berea Sandstone. The rock has been removed by dissolution in acid. The minimum apparent diameter of a throat (T) and the maximum apparent diameters of two connected pores (P_1 and P_2) are shown.

are sensitive to the arrangement of pores and throats (Morrow, 1971; Chatzis *et al.*, 1983; Li *et al.*, 1986).

Pore-throat structures may consist of pores of differing sizes randomly arranged in a network and connected by throats, all of which are smaller than the smallest pore. Such pore-throat structures are defined as uncorrelated (Figure 2A). Alternatively, there may be a relationship between the sizes of pores and the sizes of the throats which connect them. These are referred to as correlated pore-throat structures. Correlated pore-throat structures can exist for systems with either spatially ordered or disordered pores. Figure 2B illustrates pores of differing sizes randomly arranged but the throat which connects a pair of neighbouring pores has a diameter which is some function of the diameters of the connected pores. Thus, there is pore-throat size correlation. Alternatively, pores can be spatially ordered such that pores of a given size tend to occur in clusters. Figure 2C illustrates a cluster of smaller pores and, since throats by definition are smaller than pores, such spatial order of pores must be accompanied by some degree of pore-throat size correlation. In structures with pore-throat size correlation, the largest throat is not necessarily smaller than the smallest pore.

The major objectives in this paper are to show that the degree of pore-throat size correlation affects the form of imbibition capillary pressure curves and that these curves provide a means of recognizing and quantifying this property.

Mohanty and Salter (1982) used a three-dimensional model in which 50% of pores have noncorrelated pore throats and 50% have directly connected throats of identical size. However, they did not consider the case where there is a correlation between the sizes of directly connected pores and throats. Chatzis and Dullien (1979) proposed a network model in which the size of the throat connecting two neighbouring pores is correlated with the size of the smaller pore. Li *et al.* (1986) proposed a model with throat sizes which are more highly

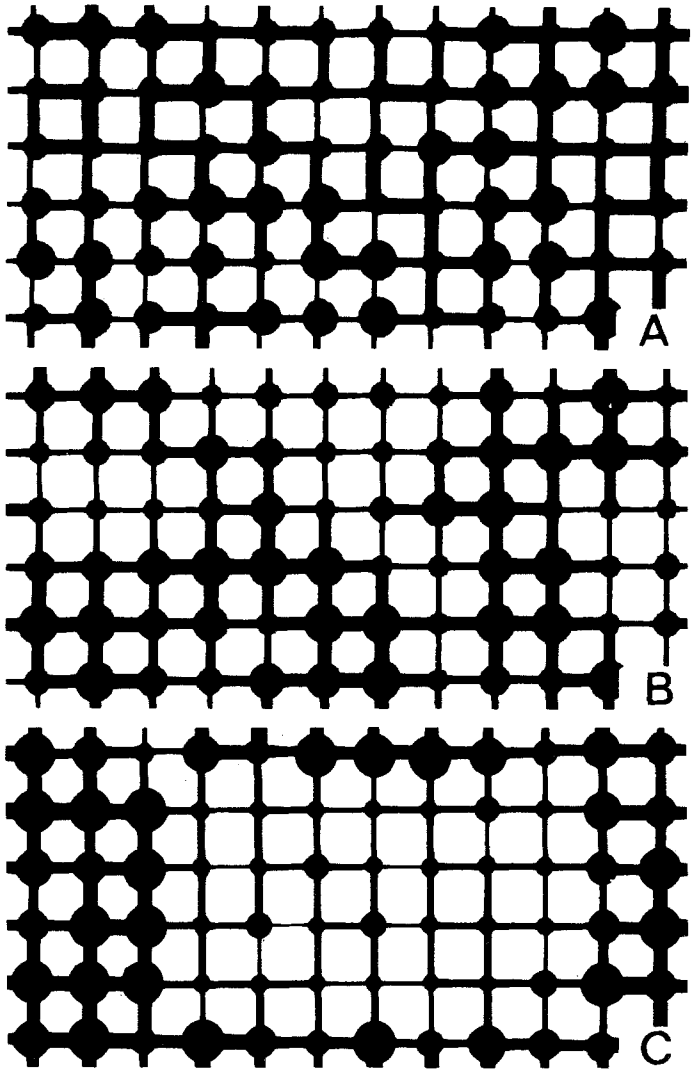

Fig. 2. Diagrammatic representation of: (A) spatially disordered pores with uncorrelated pore-throat sizes; (B) spatially disordered pores with correlated pore-throat sizes; (C) spatially ordered pores with correlated pore-throat sizes.

correlated with pore sizes than the model of Chatzis and Dullien, since the size of a throat has a relationship to the size of the two pores which it connects.

Computer simulations of drainage-imbibition processes showed that breakthrough pressures and saturations, the critical end points of wetting-phase and nonwetting-phase saturation, in drainage and imbibition respectively, and the form of simulated relative permeability curves all were significantly different for uncorrelated and correlated pore-throat models. Since these models were identical, except for the arrangement of throats in relation to pores, the degree of

pore-throat correlation appears to be an important property influencing flow and fluid displacement.

Experimentally determined capillary pressure curves for Berea Sandstone and Indiana Limestone exhibit characteristics of computer simulated capillary pressure curves for uncorrelated and correlated pore-throat structures respectively. Observation of pores and throats occupied by invading nonwetting phase (Wood's metal), at several pressures, provides direct evidence consistent with the interpretations made from the capillary pressure curves. We conclude that rocks display varying degrees of pore-throat correlation and that this is an important property affecting two phase fluid displacement precesses which has received little attention in the published literature. Degree of pore-throat correlation is a property which is difficult to quantify by direct observation but which can be estimated from capillary pressure curves.

The shapes of mercury injection (drainage) and withdrawal (imbibition) capillary pressure curves are influenced by the sizes, shapes, arrangement and interconnectedness of pores and throats. Lenormand *et al.* (1983), Li and Wardlaw (1986a and b), Chen (1986) and Li *et al.* (1986) discuss the principles which govern the 'decisions' of interfaces to move from one point to another, to enter or to leave a pore or throat. These principles formed the basis of computer programs to simulate drainage and imbibition processes for pore-throat networks with specified properties (e.g., pore and throat sizes, number of throats connecting with each pore, degree of pore-throat size correlation, etc.) Capillary pressure curves for rock samples can be compared with the computer simulated curves for known structures. Such comparisons provide a basis for inferring some aspects of the pore structure of rock samples.

2. Materials and Methods

2.1. COMPUTER SIMULATED CAPILLARY PRESSURE CURVES

The sequence of events contained in the computer programs which were used to simulate drainage and imbibition are outlined and summarized in Appendix A of Li *et al.* (1986).

Uniform size interval distributions are used for pores and throats, for comparative purposes, but can be transformed to any selected size-frequency distribution.

The two computer simulated curves which appear as Figures 3 and 4 are for three-dimensional networks with the following properties:

(a) Six throats connect with every pore.
(b) The shapes of all pores and throats are constant and independent of size.
(c) The total volume of throats is small compared with pores and can be neglected to a first approximation.

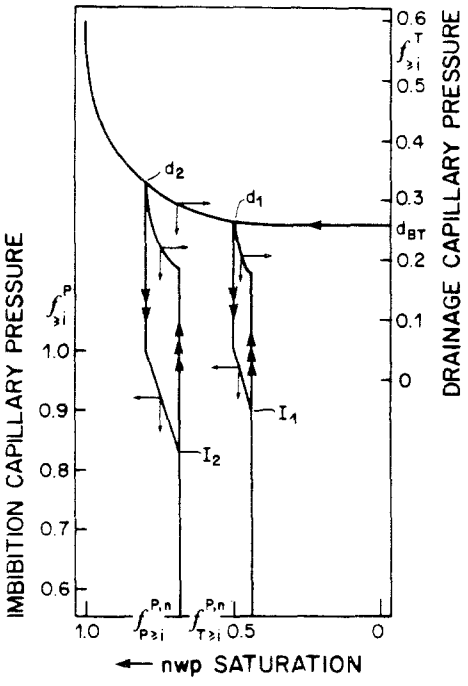

Fig. 3. Computer simulation of capillary pressure curves for uncorrelated pore-throat structure; primary drainage curve (one arrow), imbibition curves (2 arrows) and secondary drainage curves (3 arrows).

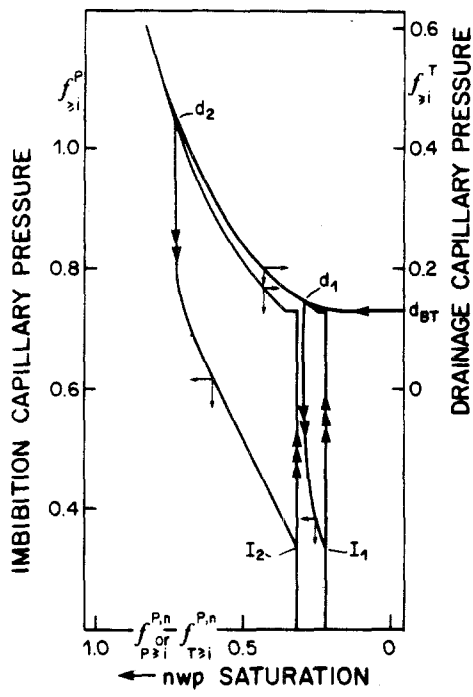

Fig. 4. Computer simulation of capillary pressure curves for correlated pore-throat structure. Arrows as in caption for Figure 3.

(d) Interfaces move by piston-type motions in both drainage and imbibition. Pores connected to a nonwetting phase (nwp) sink empty completely at an imbibition pressure related to pore diameter except for pores which have all directly connected throats occupied by nwp and these do not empty (Li and Wardlaw 1986b). Snap-off in throat events are not included (Li and Wardlaw, 1986a and b).

(e) The products of interfacial tension and cosine of contact angle are not necessarily equal during drainage and imbibition but values for all drainage curves are assumed to be identical as are values for all imbibition curves.

In both computer models the pores are randomly arranged, with respect to each other, in the networks. However, in the case of the uncorrelated pore-throat structure, the throats are arranged in a random manner without relation to the sizes of the adjacent pores. In the case of the correlated structure, a throat diameter (D^T) directly connecting a pair of neighbouring pores of diameters D_1^P and D_2^P is a function of the diameters of these pores. The function is the product of adjacent pore diameters expressed as a fraction of the largest pore diameter $D^P_{\max}$. That is

$$D^T = (D_1^P \cdot D_2^P)/D_{\max}^P.$$

Throats in the pore-throat correlated models which are assigned sizes using this relationship form a nonuniform size distribution even though the pore size distribution is uniform. However, the set of required throat sizes is known and reassignment of the boundaries of this throat distribution to give a uniform distribution is easily accomplished (Li *et al.*, 1986). Thus, the pore and throat size distributions for the uncorrelated and correlated models are identical and these models differ only in the arrangement of throats with respect to pores.

A full discussion of the notation used in Figures 3 and 4 is given in Li *et al.* (1986) and is discussed only briefly here. As pressure is increased during drainage (nonwetting phase displacing wetting phase) larger throats tend to be invaded before smaller throats. Invasion is not strictly according to size because of the requirements for fluid continuity. During imbibition (wetting phase displacing nonwetting phase), wp tends to displace nwp in a sequence of increasing pore size as pressure is decreased. However, a necessary condition for such displacements is that wp and nwp have continuity from the pore in question to the wp source and nwp sink respectively.

Interval distributions are useful in representing drainage and imbibition processes because events occur in a sequence related to relative size of throats and pores. The successive size intervals from smallest to largest, for throats or pores, are designated by subscripts $1, 2, 3 \ldots k$. The subscript i is used for any one of these size intervals 1 to k. The simulations reported are for uniform frequency distributions of pores and throats. For a uniform distribution of throats with k intervals, the accumulations take the form

$$f_{\geq i}^T = (k - i + 1)/k$$

The values taken by $f_{\geq i}^T$ decrease as i increases; hence $f_{\geq i}^T$ has its maximum value when referring to the smallest throat size interval $i = 1$. Consequently $f_{\geq i}^T$ parallels the increase in capillary pressure and can be used to characterize capillary pressure in a drainage process. In an analogous way, $f_{\geq i}^P$ is the fraction of pores with diameters equal to or greater than pores of diameter i. Since the function $f_{\geq i}^P$ is a maximum for the smallest pores, its decrease parallels the imbibition capillary pressure (Figures 3 and 4).

The symbol $f_{T \geq i}^{P,n}$ represents the fraction of pores (P) occupied by nonwetting phase (n) when throats (T) equal to or larger than i have been invaded during drainage. Since the assumption was made that all of the volume is associated with the pores, $f_{T \geq i}^{P,n}$ parallels the increase in nonwetting phase-saturation during drainage. Similarly, $f_{P \geq i}^{P,n}$ parallels the nonwetting-phase saturation during imbibition (Figures 3 and 4).

2.2. EXPERIMENTAL CAPILLARY PRESSURE CURVES

A Ruska mercury-injection capillary pressure apparatus (Model 1057) was used. An outline of the operating procedure is given by Purcell (1949) and in Wardlaw and Taylor (1976).

A pressure-volume correction curve is established for the apparatus by making a run without a sample in the chamber as pressure is first increased and then decreased. The volume readings obtained during a sample run are then corrected by making appropriate subtractions determined on the blank run at corresponding pressures. In this way, compression effects and the effects of forcing mercury into small spaces in the interior of the instrument are eliminated.

2.3. WOOD'S METAL POROSIMETRY

Wood's metal porosimetry is discussed by Dullien (1981), Dullien and Dhawan (1975), and Swanson (1979). The apparatus used was similar to that described by Swanson (1979) and involved the injection of molten alloy (mp $\cong$ 70°C) into a rock sample at a known capillary pressure. This pressure was maintained and the sample was cooled causing solidification of Wood's metal. The procedure is repeated for several different capillary pressures and the pores and throats

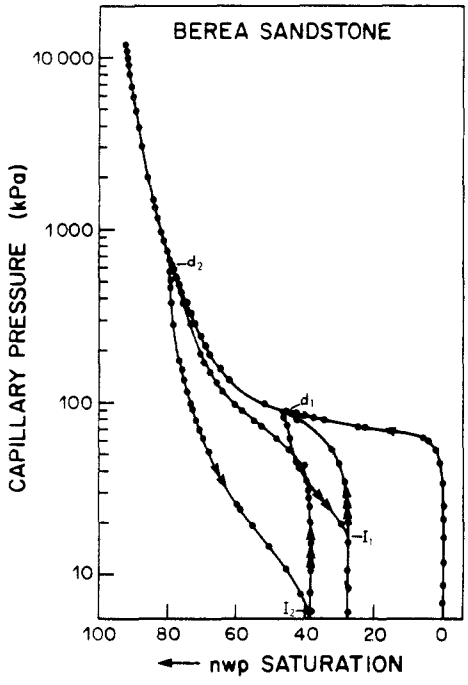

Fig. 5. Experimental mercury capillary pressure curves for Berea Sandstone. Arrows as in caption for Figure 3.

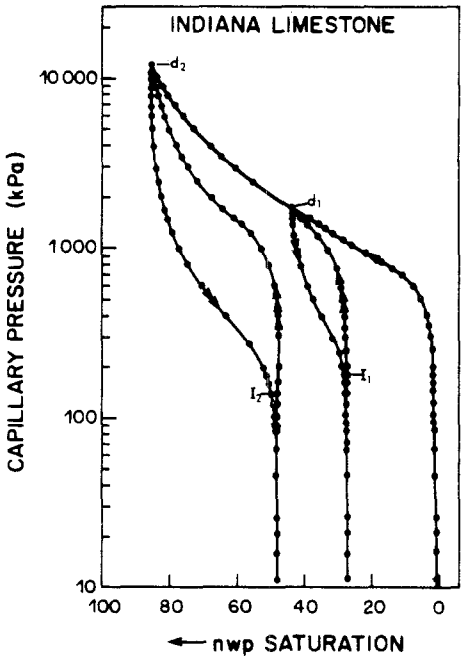

Fig. 6. Experimental mercury capillary pressure curves for Indiana Limestone. Arrows as in caption for Figure 3.

Table I. Direct measurements of apparent sizes of pores and throats occupied by Wood's metal at various capillary pressures and inferred saturations

Wood's metal invasion pressure (kPa)	Inferred Wood's metal saturation (% pore volume)	Minimum throat diam. penetrable with Wood's metal (μm)	Measured throat diam. (μm)			Measured pore diam. (μm)			Number of pores plus throats measured	Correlation coefficient for pore and throat sizes (R^2)
			Min.	Max.	Av.	Min.	Max.	Av.		
Berea Sandstone										
269	73	7	4	64	24	29	345	176	400	0.14
448	78	4	4	64	21	46	346	154	400	0.14
3548	90	0.5	3	70	19	26	406	159	400	0.18
Indiana Limestone										
861	30	2	2	34	11	7	185	64	100	0.87
1481	50	1.3	2	46	8	8	163	29	100	0.94
11 989	94	0.2	0.5	20	3	2	136	10	240	0.93

invaded at each pressure can be measured. Dullien and Dhawan (1975) concluded that Wood's metal and mercury have similar $\gamma \cos \theta$ terms (γ = surface tension, θ = contact angle) in the Young–Laplace equation of capillarity. With this assumption, the known capillary pressures of invasion for Wood's metal can be equated with Wood's metal saturations by using the mercury capillary pressure curve for the same sample (Figures 5 and 6). Values of capillary pressure and saturation are recorded in Table I.

Following solidification, two slices were cut from the invaded core. One was chemically etched to remove the rock and expose Wood's metal in relief. Dilute hydrochloric acid was used to dissolve carbonate and 1-to-1 concentrated hydrofluoric acid-water used to dissolve sandstone. The other slice was impregnated with fluorescent epoxy to saturate pore space not invaded by Wood's metal. This sample was then cut and polished for viewing in reflected ultraviolet light.

2.4. MEASUREMENT OF PORE AND THROAT SIZES

Indiana Limestone has many pores and throats which are too small to be measured satisfactorily with an optical microscope. For this reason and for consistency, all measurements for Indiana Limestone and Berea Sandstone were made on enlarged scanning electron photomicrographs of samples impregnated with Wood's metal and subsequently etched so that Wood's metal stands in relief.

The sizes of pores and throats in Berea Sandstone were apparent diameters measured at the plane of the cut and polished surface of the etched sample. These apparent diameters were minimum diameters measured at throats and maximum diameters measured in connected pores as illustrated in Figure 1. For each throat measured, two directly connected pores also were measured. All measurements were made on enlarged photographs using a scale graduated in millimeters.

In Indiana Limestone, the same methods were used but for the smallest pores and throats it was more difficult to determine if these were at the cut and polished surface or slightly below this surface. In the latter case, the pore and throat measurements are not all made on a two-dimensional surface but include measurements of apparent sizes seen with the third dimension exposed. This will cause the sizes of the smallest pores and throats to be slightly larger than if the measurements had been made on a planar surface.

3. Results

3.1. COMPUTER SIMULATED CAPILLARY PRESSURE CURVES

Figures 3 and 4 present the results of computer simulations of primary drainage, imbibition and secondary drainage for the uncorrelated and correlated pore-throat models previously described.

Comparing the simulated capillary pressure curves for the uncorrelated and correlated pore-throat models, the drainage curve has a higher breakthrough pressure ($\int_{\geq i}^{T}$) for the uncorrelated model (compare d_{BT} in Figures 3 and 4) and ascends less steeply (d_{BT} to d_2) than for the correlated structure. These characteristics are implicit and can be compared only where the pore sizes and throat sizes have been translated to uniform distributions.

Other critical differences between these models can be recognized for any size distribution of throats and pores. For the uncorrelated model, the end points of two imbibition curves terminate at different pressures (I_1 and I_2, Figures 3 and 5) and the breakthrough pressures on the secondary drainage curves are lower than the breakthrough pressure on the primary drainage curve (d_{BT}). For the correlated model, the end points of two imbibition curves terminate at approximately the same pressures (I_1 and I_2, Figures 4 and 6) and breakthrough pressures on the secondary drainage curves are the same as the breakthrough pressure on the primary drainage curve (d_{BT}).

A further difference between the uncorrelated and correlated models is seen on the simulated curves (Figures 3 and 4) but not on the experimental curves. For the correlated model, the difference in saturation at the end points of two imbibitions is equal to the difference in saturation between the starting point of the first imbibition curve and the point on the second secondary drainage curve at the same pressure. This is not the case for the uncorrelated model.

3.2. EXPERIMENTAL CAPILLARY PRESSURE CURVES

The imbibition capillary pressure curves for Berea Sandstone (Figure 5) resemble those of the simulation for the uncorrelated pore-throat model (Figure 3). The end points of the imbibition curves are at lower pressures for imbibition initiated at higher nwp saturations (I_1 and I_2, Figure 5). Also, the breakthrough pressures for the secondary drainage curves are lower than for the primary drainage curve.

The imbibition capillary pressure curves for Indiana Limestone (Figure 6) resemble those of the simulation for the correlated pore-throat model (Figure 4) in that the end points of the two imbibition curves terminate at approximately the same pressure (I_1 and I_2, Figure 6). The breatkthrough pressures for the secondary drainage curves are similar to the primary drainage curves.

3.3. DIRECT MEASUREMENT OF PORE AND THROAT STRUCTURES

Figures 7 and 8 illustrate etched samples of Berea Sandstone at Wood's metal saturations of 73% and 90% of pore volume (Table I). Observation of thin sections in combination with these etched impregnations of Wood's metal show that most of the porosity is interparticle and associated with quartz grains. However, there is some intraparticle micro-porosity in partially dissolved grains

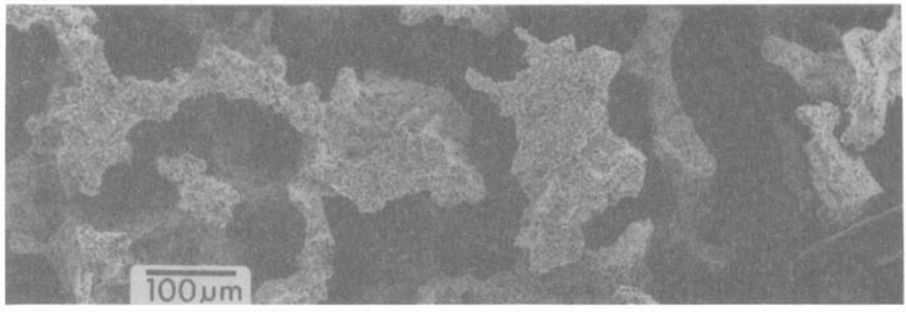

Fig. 7. Wood's metal occupying 73% of the pore volume in Berea Sandstone. Rock removed by dissolution in acid.

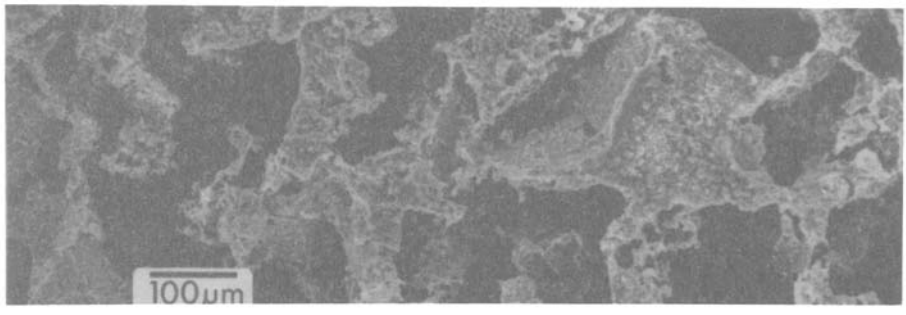

Fig. 8. Wood's metal occupying 90% of the pore volume in Berea Sandstone. Rock removed by dissolution in acid.

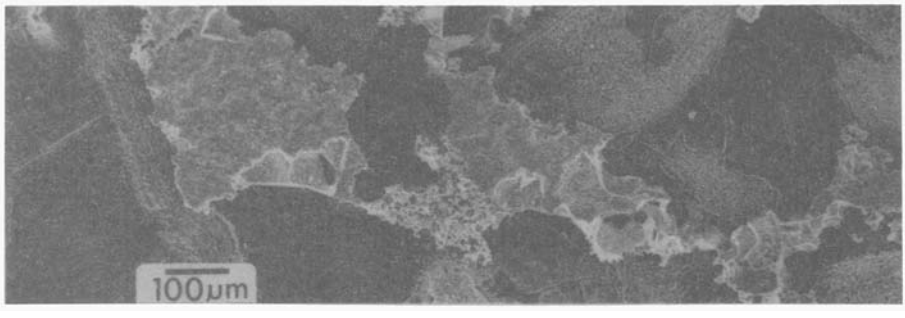

Fig. 9. Wood's metal occupying 30% of the pore volume in Indiana Limestone. Rock removed by dissolution in acid.

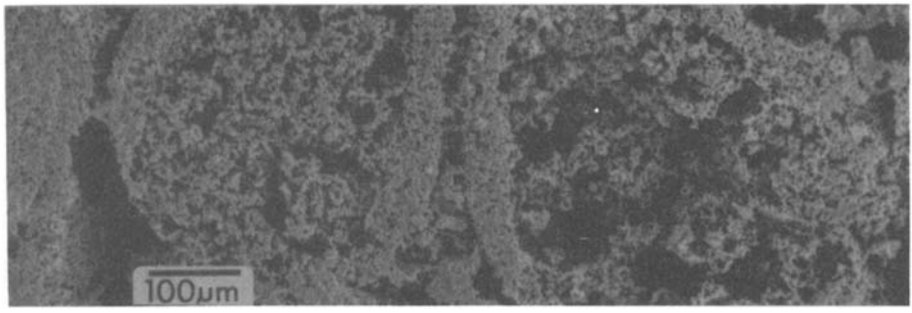

Fig. 10. Wood's metal occupying 94% of the pore volume in Indiana Limestone. Rock removed by dissolution in acid.

of micro-crystalline silica and feldspar and minor micro-porosity associated with kaolinite in the matrix.

At successively higher capillary pressures, Wood's metal is forced into smaller throats and into the 'nooks and crannies' of pore walls and the outlines of Wood's metal became more irregular (Figure 8).

Figures 9 and 10 of samples of Indiana Limestone at Wood's metal saturations of 30% and 94% of pore volume (Table I). Observations of thin sections and the

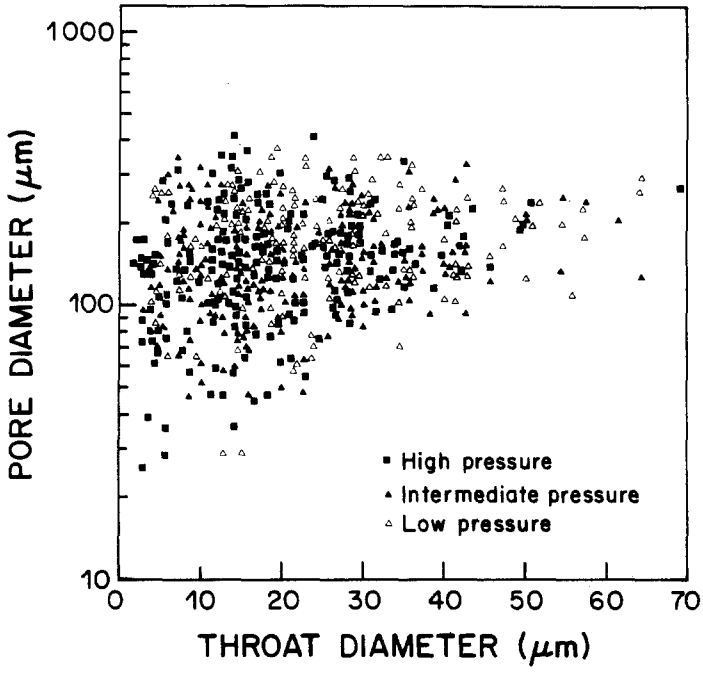

Fig. 11. Minimum apparent throat diameters versus the average maximum apparent diameters for two directly connected pores (see Figure 1) in Berea Sandstone at three different capillary pressures and Wood's metal saturations.

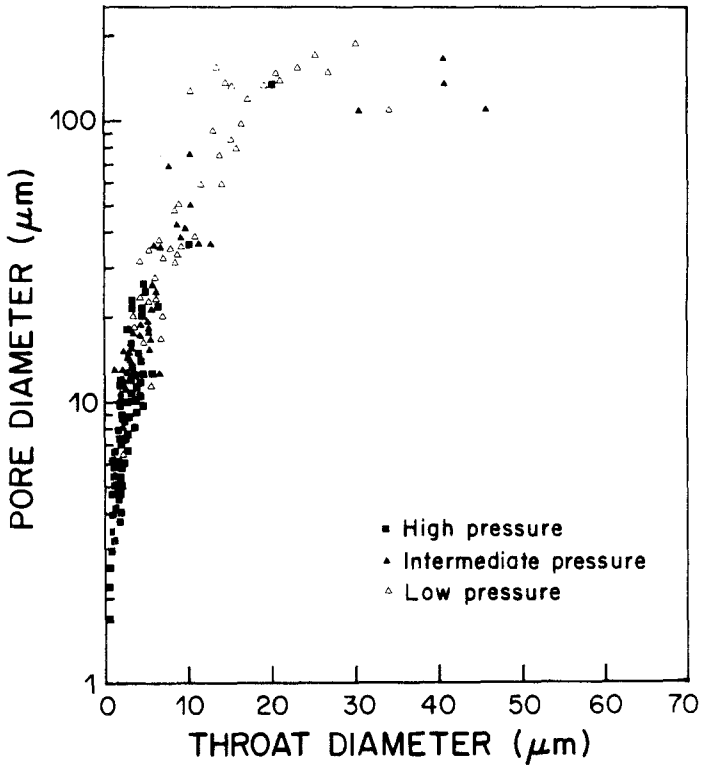

Fig. 12. Minimum apparent throat diameters versus the average maximum apparent diameters for two directly connected pores in Indiana Limestone at three different capillary pressures and Wood's metal saturations.

Wood's metal impregnated samples show that there are large interparticle pores but also abundant intra-particle micro-porosity associated with micro-crystalline carbonate grains. Microporosity constitutes a much larger proportion of the total pore volume than in Berea Sandstone.

Measurements of pore and throat sizes were made from large photographs of which Figures 7 to 10 are small portions. A summary of measurements of minimum, maximum and average throat and pore sizes for each invasion capillary pressure is given in Table I. For each apparent throat diameter measurement there are two apparent diameters of directly connected pores and these were averaged. These throat and averaged pore measurements are shown graphically for Berea Sandstone and Indiana Limestone on Figures 11 and 12 and correlation coefficients given in the final column of Table I. The low values of correlation coefficients for Berea Sandstone indicate little correlation between pore sizes and the sizes of connecting throats whereas the high values for Indiana Limestone indicate a correlated pore-throat structure. These relationships also are apparent from Figures 11 and 12.

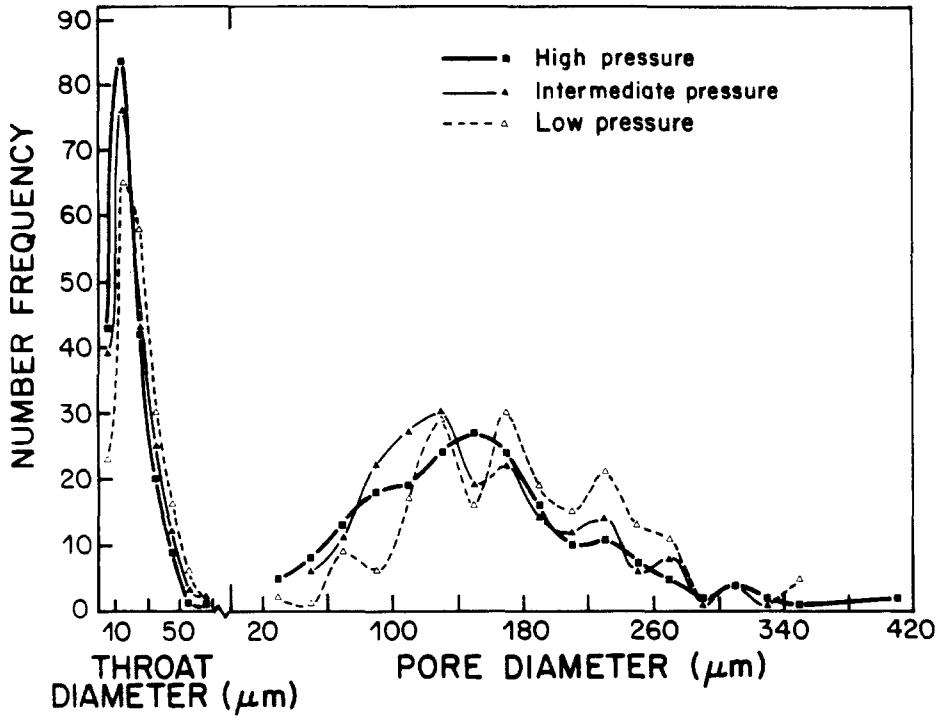

Fig. 13. Size-frequency distribution of pores and throats, in Berea Sandstone, occupied by Wood's metal at three different capillary pressures. Data as in Figure 11 plotted in different format.

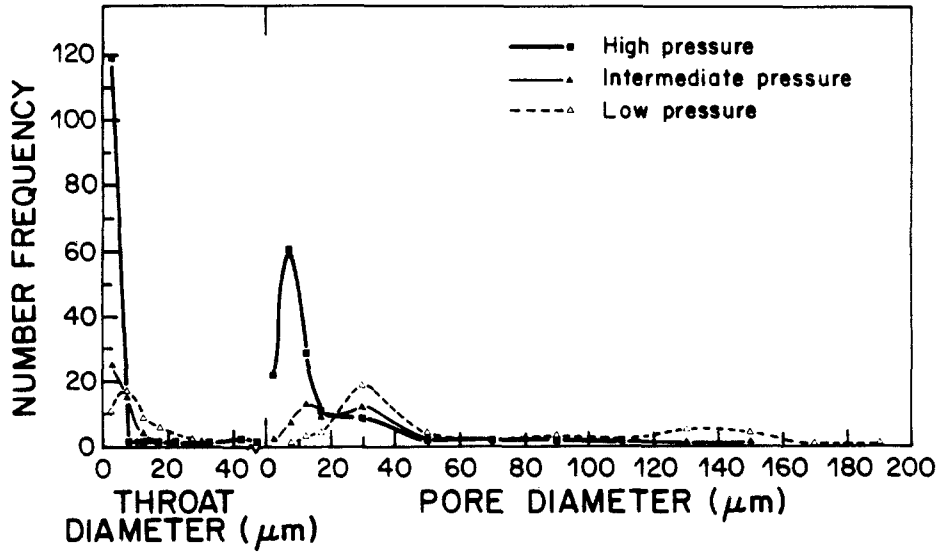

Fig. 14. Size-frequency distribution of pores and throats, in Indiana Limestone, occupied by Wood's metal at three different capillary pressures, Data as in Figure 12 plotted in different format.

Figures 13 and 14 depict these data as size-frequency plots for pores and throats occupied at three invasion capillary pressures for Berea Sandstone and Indiana Limestone respectively. For Berea Sandstone, while the frequency of smaller throats filled increases with invasion pressure, additional large pores as well as small pores are filled at higher pressures (Figure 13). In Indiana Limestone, at higher capillary pressures, the frequency of both small throats and small pores filled by Wood's metal increases abruptly (Figure 14).

4. Discussion

The different relative positions of the end points I_1 and I_2 (Figures 3 and 4) on the computer simulations of imbibition capillary pressure curves, for the uncorrelated and correlated pore-throat models, can be understood in terms of throat size and pore size controlled domains as given in Li *et al.* (1986).

During drainage, it is assumed that if a throat is occupied by nwp any connected pore also will be filled. As capillary pressure is increased, smaller throats become invadeable with nwp until a point is suddenly reached at which a connected path of throats occupied by nwp extends from one edge of a finite grid to the other. This is referred to as a breakthrough (BT) and the domain of throats and connected pores which is occupied by nwp is referred to as an infinite, large throat domain (I, LTD, Li *et al.*, 1986). In this domain, pores are being classified according to the size of the throats to which they are connected.

In imbibition, domains are controlled by pore size and withdrawal of nwp from pores is accompanied by nwp withdrawal from directly connected throats. Wetting phase penetrates small pores before large pores. An imbibition end point is reached at a pressure and nwp saturation such that an infinite large pore domain (I, LPD) no longer exists. That is, a continuous pathway of nwp no longer exists from source to sink.

For a model with perfect pore-throat correlation, the domain of pores and throats which is occupied by nwp at breakthrough in drainage persists intact during imbibition until the moment when nwp continuity is finally broken. This means that imbibition curves initiated at different saturations (d_1 and d_2) will end at the same pressure as is seen for points I_1 and I_2 on Figures 4 and 6.

The essence of the correlated pore-throat structure is that the filling of the larger throats with nwp in drainage is accompanied by the filling of the larger pores and, conversely, the emptying of the larger pores is accompanied by nwp withdrawal from the larger throats.

This is not the case in the uncorrelated pore-throat model where there is no relationship between the sizes of throats and the sizes of the pores which they connect. Thus, during all stages of drainage, pores of all sizes are filled in a random manner. Although the total number of pores occupied by nwp is greater at d_2 than at d_1 (Figure 3), at both d_1 and d_2 the relative frequency of pores occupied by nwp in all size categories is equal. However, nwp withdraws in an

order of increasing pore size and, for imbibition commencing at a higher saturation (d_2), a large fraction of the pores occupied by nwp can be emptied before nwp becomes disconnected. It follows that the pore size emptying at the imbibition end point (I_2) will be larger than at the imbibition end point I_1 (Figure 3). For this reason, imbibition initiated at higher nwp (d_2), in uncorrelated pore-throat models, causes an imbibition end point (I_2) which is at a lower imbibition pressure. More specific information is given in Li *et al.* (1986).

In the correlated pore-throat model, breakthrough pressures are similar for the primary and for the secondary drainage curves (Figures 4 and 6). Breakthrough pressures for secondary drainage curves are not affected by residual nwp saturation because the infinite large pore domain (I, LPD), which exists just prior to the imbibition end point, resembles the infinite large throat domain (I, LTD) at breakthrough in drainage.

This is not the case for the uncorrelated pore-throat model where the residual nwp at the end of imbibition contributes to the reconnection of nwp in secondary drainage. In this case, nwp continuity is established at a lower pressure in secondary drainage than in primary drainage (Figures 3 and 5).

Continuous and discontinuous nwp can be obtained at any pressure or saturation from the computer simulations and this facilitates understanding differences between correlated and uncorrelated pore-throat models. In correlated models, nwp saturation during secondary drainage is the sum of the saturation at the same pressure during primary drainage and a component of residual nwp not yet reconnected by nwp advancing in secondary drainage. The component of residual nwp associated with the drainage saturation increment between d_1 and d_2 will not be reconnected with continuous nwp until the second secondary drainage curve reaches a pressure equivalent to d_1. This is not the case in the uncorrelated pore-throat model.

The relative positions of the end points of the imbibition capillary pressure curves and the relative positions of the breakthrough pressures for primary and secondary drainage curves obtained experimentally for Berea Sandstone (Figure 5) and Indiana Limestone (Figure 6) resemble those obtained by computer simulation for the uncorrelated and correlated pore-throat models respectively.

Direct measurements of throat and pore sizes invaded by Wood's metal show that Indiana Limestone has a strong component of pore-throat size correlation (Figure 12) with correlation coefficients (R^2) of 0.87, 0.94, and 0.93 at three successively higher capillary pressures (Table I). Similar measurements for Berea Sandstone show no obvious correlation (Figure 11). Correlation coefficients (R^2) of 0.14, 0.14 and 0.18 (Table I) at three different capillary pressures indicate the prevailing disordered arrangement of throats with respect to pores. These results provide evidence that degree of pore-throat size correlation is a property which can be evaluated from the relative pressures of the end points of imbibition curves initiated at different wp saturations.

Examination of Wood's metal impregnated samples and thin sections show that

intra-particle micro-porosity, which is associated with micro-crystalline particles, is abundant in Indiana Limestone and is the cause of spatial ordering of pore sizes. Micro-pores are strongly clustered as local domains (Figure 10). Some local clustering of micro-pores also occurs in Berea Sandstone but is of limited extent. Since throats by definition are smaller than pores, spatial ordering of pores will be accompanied by pore-throat size correlation (Figure 2C). However, the converse is not true. That is, spatial disorder of pores does not exclude the possibility of pore-throat correlation (Figure 2B).

The results for Berea Sandstone reported here are consistent with those of Dullien and Dhawan (1975) and Dullien (1979), who reported the results of combined Wood's metal porosimetry, photomicrography and theoretical analysis of nwp penetration in Berea Sandstone. At low and intermediate capillary pressures, they reported that there is no simple relationship between pore size and throat size and that the behaviour of the system is as with randomly distributed capillaries. However, at the highest capillary pressure, it appeared that the pore sizes may not have been completely randomly distributed. In a more recent study, Yanuka *et al.* (1986) use a random packing of ellipsoids to represent the pore space of Berea Sandstone.

Li *et al.* (1986) have shown in computer simulations that pore-throat size correlation is a property which affects the efficiency of two phase displacement processes and the form of relative permeability curves. Morrow (1971) and Chatzis *et al.* (1983) showed that ordering of particles affects the magnitudes of the critical end point saturations in drainage and imbibition. These studies show that it is not just the sizes of pores and throats which affect fluid movements and displacement efficiency within porous materials, but the manner in which pores and throats of different sizes are arranged relative to each other.

5. Conclusions

(1) Correlated and uncorrelated pore-throat structures occur in rocks.
(2) The shapes of relative permeability curves and displacement efficiency are sensitive to degree of pore-throat size correlation.
(3) Degree of pore-throat size correlation is a property which is difficult to quantify by direct observation but which can be evaluated from capillary pressure curves.

Acknowledgements

Funds for this project were provided by the Alberta Oil Sands Technology Research Authority (AOSTRA) and are gratefully acknowledged. We also thank Mr M. McKellar, Department of Geology and Geophysics, who assisted with various phases of this work.

References

Bell, W. K., Van Brakel, J., and Heertjes, P. M., 1981, Mercury penetration and retraction hysteresis in closely packed spheres, *Powder Tech.* **29**, 75–88.

Chatzis, I. and Dullien, F. A. L., A network approach to analyze and model capillary and transport phenomena in porous media, in J. Ganoulis, (ed.), *Comptes Rondus Symposium de l'AIRH*, Thessaloniki, Greece, 1979, pp. 1.2–1.22.

Chatzis, I., Morrow, N. R., and Lim, H. T., 1983, Magnitude and detailed structure of residual oil saturation, *Soc. Pet. Eng. J.* **23**, 311–326.

Chen, J. D., 1986, Some mechanisms of immiscible fluid displacement in small networks, *J. Coll. Interface Sci.* **110**, 488–503.

Dullien, F. A. L., 1979, *Porous Media: Fluid Transport and Pore Structure*, Academic Press, New York, pp. 75–136.

Dullien, F. A. L., 1981, Wood's metal porosimetry and its relation to mercury porosimetry, *Powder Tech.* **29**, 109–116.

Dullien, F. A. L. and Dhawan, G. K., 1975, Bivariate pore-size distribution of some sandstones, *J. Coll. Interface Sci.* **52**, 129–135.

Lenormand, R., Zarcone, C., and Sarr, A., 1983, Mechanisms of the displacement of one fluid by another in a network of capillary ducts, *J. Fluid Mech.* **135**, 337–353.

Li, Y. and Wardlaw, N. C., 1986a, The influence of wettability and critical pore-throat size ratio on snap-off, *J. Coll. Interface Sci.* **109**, 461–472.

Li, Y. and Wardlaw, N. C., 1986b, Mechanisms of nonwetting phase trapping during imbibition at slow rates, *J. Coll. Interface Sci.* **109**, 473–486.

Li, Y., Laidlaw, W. G., and Wardlaw, N. C., 1986, Sensitivity of drainage and imbibition to pore structures as revealed by computer simulation of displacement process, *Adv. Coll. Interface Sci.* **26**, 1–68.

Mohanty, K. K. and Salter, S. J., Multiphase flow in porous media: II. Pore-level modeling, *S.P.E. 11018*, 57th Annual Technical Conference, Dallas, 1982, pp. 1–21.

Morrow, N. R., 1971, Small-scale packing heterogeneities in porous sedimentary rocks, *AAPG Bull.* **55**, 514–522.

Purcell, W. R., 1949, Capillary pressure – their measurement using mercury and the calculation of permeability therefrom, *J. Petr. Tech.* **1**, 39–48.

Purcell, W. R., 1950, Interpretation of capillary pressure data, *Petr. Trans. AIME* **189**, 369–371.

Swanson, B. F., 1979, Visualizing pores and nonwetting phase in porous rocks, *J. Petr. Tech.* **31**, 10–18.

Wardlaw, N. C. and Taylor, R. P., 1976, Mercury capillary pressure curves and the interpretation of pore structure and capillary behavior in reservoir rocks, *Bull. Can. Petr. Geol.* **24**, 225–262.

Winslow, D. N. and Lovell, C. W., 1981, Measurements of pore size distributions in cements, aggregates and soils, *Powder Tech.* **29**, 151–165.

Yanuka, M., Dullien, F. A. L., and Elrick, D. E., 1986, Percolation processes and porous media, *J. Coll. Interface Sci.* **112**, 24–41.